Neuro-Oncology

22(10), 1495–1504, 2020 | doi:10.1093/neuonc/noaa101 | Advance Access date 17 April 2020

A combined approach of convection-enhanced delivery of peptide nanofiber reservoir to prolong local DM1 retention for diffuse intrinsic pontine glioma treatment

Vanessa Bellat,[†] Yago Alcaina,[†] Ching-Hsuan Tung, Richard Ting, Adam O. Michel, Mark Souweidane, and Benedict Law

Molecular Imaging Innovations Institute, Department of Radiology, Weill Cornell Medicine, New York, New York (V.B., Y.A., C-H. T., R. T., B.L.); Laboratory of Comparative Pathology, Center of Comparative Medicine and Pathology, Memorial Sloan Kettering Cancer Center, The Rockefeller University, Weill Cornell Medicine, New York, New York (A.O.M); Department of Neurological Surgery, New York-Presbyterian Hospital, Weill Cornell Medicine, New York, New York (M.S.)

Corresponding Author: Benedict Law, PhD, 413 East 69th Street, New York, NY, 10021, USA (sbl2004@med.cornell.edu).

[†]Vanessa Bellat and Yago Alcaina contributed equally to this work.

Abstract

Background. Diffuse intrinsic pontine glioma (DIPG) is a highly lethal malignancy that occurs predominantly in children. DIPG is inoperable and post-diagnosis survival is less than 1 year, as conventional chemotherapy is ineffective. The intact blood–brain barrier (BBB) blocks drugs from entering the brain. Convection-enhanced delivery (CED) is a direct infusion technique delivering drugs to the brain, but it suffers from rapid drug clearance. Our goal is to overcome the delivery barrier via CED and maintain a therapeutic concentration at the glioma site with a payload-adjustable peptide nanofiber precursor (NFP) that displays a prolonged retention property as a drug carrier.

Methods. The post-CED retention of ^{89}Zr-NFP was determined in real time using PET/CT imaging. Emtansine (DM1), a microtubule inhibitor, was conjugated to NFP. The cytotoxicity of the resulting DM1-NFP was tested against patient-derived DIPG cell lines. The therapeutic efficacy was evaluated in animals bearing orthotopic DIPG, according to glioma growth (measured using bioluminescence imaging) and the long-term survival.

Results. DM1-NFP demonstrated potency against multiple glioma cell lines. The half-maximal inhibitory concentration values were in the nanomolar range. NFP remained at the infusion site (pons) for weeks, with a clearance half-life of 60 days. DM1-NFP inhibited glioma progression in animals, and offered a survival benefit (median survival of 62 days) compared with the untreated controls (28 days) and DM1-treated animal group (26 days).

Conclusions. CED, in combination with DM1-NFP, complementarily functions to bypass the BBB, prolong drug retention at the fusion site, and maintain an effective therapeutic effect against DIPG to improve treatment outcome.

Key Points

1. Using peptide nanofiber as a drug delivery platform prolongs the drug retention after CED.
2. DM1-loaded nanofiber increases survival of orthotopic DIPG xenograft mouse models compared with the free drug.

Importance of the Study

DIPG is an inoperable and incurable cancer, and there is no effective chemotherapy. An intact BBB and rapid drug clearance from the brain limit the effectiveness of any systemic drug treatments. A combination of CED (a direct infusion technique) and NFP (a drug carrier with a prolonged retention property) circumvents these limitations. For the first time, we showed that CED of DM1-loaded NFP (DM1-NFP) prolonged survival in DIPG-bearing mice compared with free DM1. This approach offered a valuable tool for treating DIPG and potentially other localized brain malignancies. The design of the NFP is flexible, allowing the incorporations of different drugs and imaging agents. An NFP approach is effective at a very low drug concentration, requires a single infusion, is clinically translatable, and could potentially limit the toxicity and treatment burden of systemically delivered drugs. This approach could rescue drug candidates previously abandoned due to poor solubility, insufficient delivery, and dose-limiting toxicity for brain cancer treatment.

Brainstem glioma comprises 10–20% of all pediatric tumors in the central nervous system (CNS). Diffuse intrinsic pontine glioma (DIPG) accounts for a majority of the cases. It is a highly infiltrative malignant glial neoplasm of the ventral pons.[1] DIPG predominantly occurs in children between the ages of 5 and 10 years old, and is associated with a median survival of 9–12 months after 2 years.[2] One reason for such a poor prognosis is that surgical glioma resection is not possible. DIPG is located in a critical area within the brain. Furthermore, there is a lack of effective drugs against DIPG. The blood–brain barrier (BBB) prevents the delivery of systemic chemotherapeutics to the brain, resulting in insufficient therapeutic concentrations for DIPG treatment.[3] Radiotherapy remains the primary treatment, but only offers a short temporal benefit for slowing down the glioma progression.[4] The disease progresses in nearly all cases.[5] Convection-enhanced delivery (CED), a direct infusion technique for delivering drugs to brain, can bypass the BBB.[6] Appealing features include high regional drug concentration and negligible systemic exposure. A major drawback of CED is that drug molecules can be rapidly cleared from the brain immediately after the delivery. For example, the local clearance half-life of panobinostat in rat brain after CED was 2.9 hours.[7] In general, larger and more hydrophobic drug molecules are known to display longer clearance time.[8] Longer infusion time, larger infusion volume, and repeated procedures using an implanted catheter have been used to compensate for the rapid clearance. Such optimizations have been mainly applied to supratentorial glioma, and may increase the risks of seizure, infection, and anatomical shifting.[9,10] For infratentorial glioma such as DIPG, precision cannula placement can be more challenging. A longer cannula is required to be inserted deeply inside the brain, which may increase the risk of injuring salient architecture. Further, increasing the infusion volume may cause anatomical deformation of the pons.[11] There is an unmet need for more effective drugs as well as less invasive approaches to maintain high drug concentrations at DIPG.

Nanoparticles have been used to prolong CED drug retention. Methotrexate has been conjugated to serum albumin-coated maghemite nanoparticles.[12] The drug-loaded particles displayed good glioma distribution and slower clearance. In addition to delivering drug molecules, chitosan-lipid nanoparticles have been used to co-deliver small interfering RNAs of epidermal growth factor receptor and galectin-1.[13] We have previously developed a peptide nanofiber precursor (NFP) platform as a drug delivery system.[14,15] NFP is composed of multiple β-sheet peptides conjugated to methoxypolyethylene glycol ($mPEG_{2000}$-KLDLKLDLKLDLK-$CONH_2$). In aqueous media, the individual peptide conjugates self-assemble into a stable single-layer structure of high aspect ratio. Nanoparticles with a high aspect ratio display better tissue penetration properties compared with the spherical counterparts.[16] The high stability of NFP allows on-demand customizations of imaging probes[17,18] and/or drugs[15] while maintaining the desired size and morphological structure. Recently, we reported that it was not only feasible to administer NFP to the brain through CED[15,19] but that NFP subsequently displays weeks-long local retention post-CED.[15] However, the therapeutic benefits of using NFP as a drug carrier have not been demonstrated.

In the present study, we employed NFP to deliver emtansine (DM1) to DIPG sites via CED. DM1 is a bioconjugatable microtubule inhibitor. It has been approved as the drug component of antibody–drug conjugates, such as T-DM1, for breast cancer treatment. DM1 has been shown to be effective against glioblastoma multiforme (GBM)[20] and has never been tested on treating DIPG. Our initial study showed that DM1 was more potent than the traditional chemotherapeutics, such as cisplatin, doxorubicin, and dasatinib, for DIPG treatment (Supplementary Figure 1). We first investigated the biodistribution of NFP labeled with zirconium-89. ^{89}Zr is a long-lived isotope with a half-life of 78 h. Incorporating ^{89}Zr into the nanofiber would allow us to investigate the initial distribution (short-term CED) and the long-term (weeks) local and systemic clearance of NFP using dynamic PET/CT imaging. We further incorporated DM1 into NFP via a cleavable disulfide linker for promoting drug release. The resulting drug-loaded NFP (DM1-NFP) showed enhanced efficacy for treating mice bearing orthotopically implanted human-derived DIPG tumors via CED compared with free DM1. This platform significantly prolonged animal survival.

Materials and Methods

Stereotaxy and CED Infusion

All experimental procedures on animals were approved by the Weill Cornell Medicine Center Institutional Animal Care

and Use Committee (#2017-0011 and #2014-0030) and were consistent with the recommendations of the American Veterinary Medical Association and the National Institutes of Health Guide for the Care and Use of Laboratory Animals. Animals were anesthetized with isoflurane and placed on an SGL M Portable Stereotactic frame (RWD Life Science). A midline incision (5 mm) was made to expose the coronal and sagittal sutures. Each animal's head was leveled within the stereotactic frame using lambda as a reference point. Using a dental drill, a 0.5 mm burr hole was made through the skull at 0.5 mm posterior and 1 mm lateral right to lambda, consistent with pons location. Nanofil Syringe (World Precision Instruments), with a 33G needle, was used for CED at 6 mm inferior to lambda. The injection flow rate (1 μL/min) was controlled using a KDS Legato 130 Pump Controller (RWD Life Science).

Pharmacokinetic and Biodistribution Study

^{89}Zr-NFP or ^{89}Zr-DFO (20 μCi, 35 μL) was administered to Balb/c mice (Jackson Laboratory) via CED injection at the rate of 1 μL/min (n = 4/group of animals). Mice were euthanized after 4 and 21 days for organ collection. The radioactivity of all organs was measured on a Wizard^2 2-Detector Gamma Counter (PerkinElmer). A reference of known activity, prepared before the injections, was used to correct the data from the radioactive decay.

PET Imaging

After CED injections of ^{89}Zr-NFP or ^{89}Zr-DFO, PET images were acquired using an Inveon μPET/CT scanner (Siemens Medical Solutions). For animals injected with ^{89}Zr-NFP, whole-body images were acquired every 4 days. For ^{89}Zr-DFO, the animal images were acquired immediately (hour 0) and 4, 8, 12, 24, and 48 h after the injections. PET/CT maximum energy projections were processed with Amide v1.0.4 and Inveon Research Workplace software. The images were corrected according to the radioactive decay. For endpoint biodistribution studies, the mice were euthanized and the tissues were harvested. The results, corrected with the radioactive decay, were expressed as percent of the infused dose per gram (ID/g) of tissue.

Survival Study

An experimental animal model was established in 11–13 week old nonobese diabetic/severe combined immunodeficiency gamma (NSG) mice (Jackson Laboratory) by implanting green fluorescent protein (GFP)/luciferase–transduced SU-DIPGIV or SF8628 cancer cells (2×10^4; 1 μL) via intracranial injection in the pons with a flow rate of 2 μL/min. Tumor progression was monitored by bioluminescence imaging. The images were acquired every 4 days using the In Vivo Xtreme imaging system (Bruker), 15 min after intraperitoneal injection of D-Luciferin-K+ salt compound (200 μL, 15 mg/mL; PerkinElmer). The images were analyzed using Bruker Molecular Imaging Software version 7.1.1. The imaging signals were corrected from the background bioluminescence. Seven days after glioma implantation, the animals were randomly assigned into 3 groups and treated with phosphate buffered saline (PBS) (control), DM1 (1 μM), or DM1-NFP (1 μM of drug content; 20 μL) via CED (1 μL/min) (n = 10/condition). The animals were further monitored in Kaplan–Meier survival studies. Animals were euthanized according to the endpoint criteria (anorexia and cachexia, >5% weight loss daily for 2 consecutive days, lack of activity, impairment of ambulation from tumor, or hunched posture) and the organs were excised and washed with PBS prior to further procedures. GraphPad Prism software was used to plot the Kaplan–Meier estimator and calculate the survival difference between groups.

Brain Histology and Immunohistochemistry

The excised brains were fixed in 4% paraformaldehyde in PBS overnight. After fixation, the tissues were kept in 70% ethanol for 48 h. They were embedded in paraffin, sectioned in 10 μm thick slices, and stained with hematoxylin and eosin (H&E) by the Electron Microscopy and Histology Core of Weill Cornell Medicine and examined by a board-certified veterinary pathologist at Memorial Sloan Kettering Cancer Center. For immunohistochemistry, sections were deparaffinized and rehydrated before incubation overnight with anti-Ki67 (Abcam), anti-DM1 (Creative Biolabs), or rabbit immunoglobulin (Ig)G (Sigma), followed by anti-rabbit IgG-peroxidase (Sigma) and 3,3′-diaminobenzidine (DAB; Sigma). High resolution images were acquired using the Aperio 9 Digital Pathology slide scanner (Leica Biosystems).

Additional Methods

Additional methods can be found in the Supplementary Methods, including reagents and supplies, peptide synthesis, conjugation of DM1 to the peptide constructs, NFP assembly, radiochemistry, cell culture, fluorescence-activated cell sorting (FACS), fluorescence microscopy, cytotoxicity assay, in vitro drug release study, and liquid chromatography–tandem mass spectrometry (LC-MS/MS) analysis of drug in the brain.

Statistical Analysis

Statistical analysis was performed using GraphPad Prism 7.0 software. Significant differences between populations were determined using a 2-tailed Student's t-test. Mann–Whitney U-test was performed to determine significant differences in bioluminescence at the area of interests between different groups, and a Wilcoxon matched-pairs signed rank test was performed to compare the evolution of the bioluminescence over time. Kaplan–Meier plots were generated for survival analysis, and their statistical significance was analyzed using the Mantel–Cox log-rank test. For pharmacokinetic studies, the results were fit into a linear or biphasic model and the different half-lives ($t_{1/2}$) calculated using a PK Solver Microsoft Excel plug-in.

Results

NFP Retention Properties in the Pons

To investigate the long-term biodistribution and clearance of NFP following CED, we synthesized imageable NFP (^{89}Zr-NFP). These nanofibers were coassembled from a mixture of Cyanine5.5-labeled, deferoxamine (DFO)-conjugated, and naïve peptide constructs in aqueous solution (Fig. 1A). The Cyanine5.5 labeling would allow us to investigate the location and distribution of NFP in brain using histology and optical imaging. On the other hand, DFO is a chelator of ^{89}Zr radioisotope with a decay half-life of 78 h (Fig. 1B). Incorporation of ^{89}Zr into the nanofibers would allow us to study the initial distribution (short-term CED) and the long-term (weeks) local and systemic clearance in real time using PET/CT imaging. Here, we first homogenized the assembled NFP into 100 nm. At this length, the nanofibers showed a prolonged retention time in brain.[19] We then confirmed with a cell viability assay that the NFP was nontoxic to normal brain cells such as astrocytes (Fig. 1C). We finally incubated the NFP with ^{89}Zr-oxalate to form the radiolabeled nanofibers (Fig. 1D), and characterized them using transmission electron microscopy (Fig. 1E).

The pons is located on the brainstem between the midbrain and the medulla, and is below the cerebellum (Fig. 2A). Prior to starting the in vivo biodistribution experiments, we performed a preliminary study to ensure the coordinate (0.5 mm posterior, 1 mm lateral right, and 6 mm inferior to lambda) that we employed would target the pons during stereotactic surgery. The successful infusion of the nanofibers was confirmed with dissection (Fig. 2B). Histology further corroborated the presence of the nanofiber (red) at the pons infusion site (Fig. 2C). Dynamic PET/CT imaging analysis revealed that ^{89}Zr-NFP remained at the point of injection (pons) for more than 3 weeks after CED (Fig. 2D and Supplementary Figure 2). CED of ^{89}Zr-NFP was also more predictable than ^{89}Zr-DFO. The local clearance kinetics of ^{89}Zr-NFP were linear, with a long $t_{1/2}$ of 60.3 days (Fig. 2E). In contrast, ^{89}Zr-DFO (positive control) was rapidly cleared from the brain within 4 h. The clearance fit into a biphasic kinetic profile, with the calculated half-life ($t_{1/2}$ α) and the terminal half-life ($t_{1/2}$ β) at 1.4 h and 41.2 h, respectively. To confirm the enhanced retention of ^{89}Zr-NFP, we further performed an endpoint biodistribution study. We found that a majority of ^{89}Zr-NFP remained in the brain after CED. More than 47% and 38% ID/g was found in situ after 4 days and 21 days, respectively (Fig. 2F). A minimal amount of NFP (off-target radioactivity) accumulated in other organs. When ^{89}Zr-DFO was used as a control, only 4% ID/g remained in brains 4 days after CED. Overall, NFP minimized the off-target delivery of ^{89}Zr-DFO (absorption by other organs) and prolonged the retention at the CED infusion site.

NFP Is an Effective Carrier of Emtansine

The local retention properties of NFP following CED prompted us to further evaluate CED's application for delivering chemotherapeutic agents for DIPG treatment. When used as a drug carrier, the weeks-long local retention of NFP after CED should offer a prolonged glioma-drug

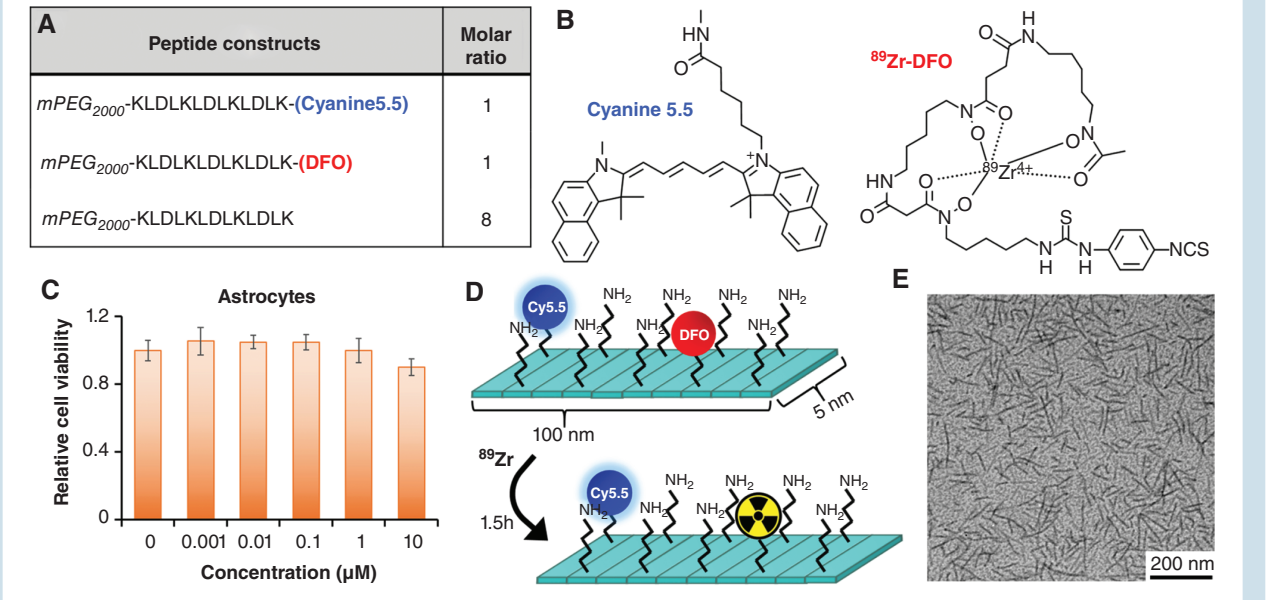

Fig. 1 The composition of a dual ^{89}Zr- and Cyanine5.5-labeled NFP. (A) The nanofiber was firstly coassembled from a mixture of Cyanine5.5-labeled, DFO-conjugated, and naïve peptide constructs, in a ratio of 1:1:8. (B) Chemical structures of Cyanine5.5 and ^{89}Zr-DFO complex. (C) Graph showing the relative cell viability of astrocyte days after incubation with different concentrations of NFP. (D) After homogenizing into 100 nm in length, ^{89}Zr was chelated to the DFO attaching on the nanofiber surface. (E) Transmission electron microscopy images (80k× magnification) of the final ^{89}Zr-NFP (15 μM).

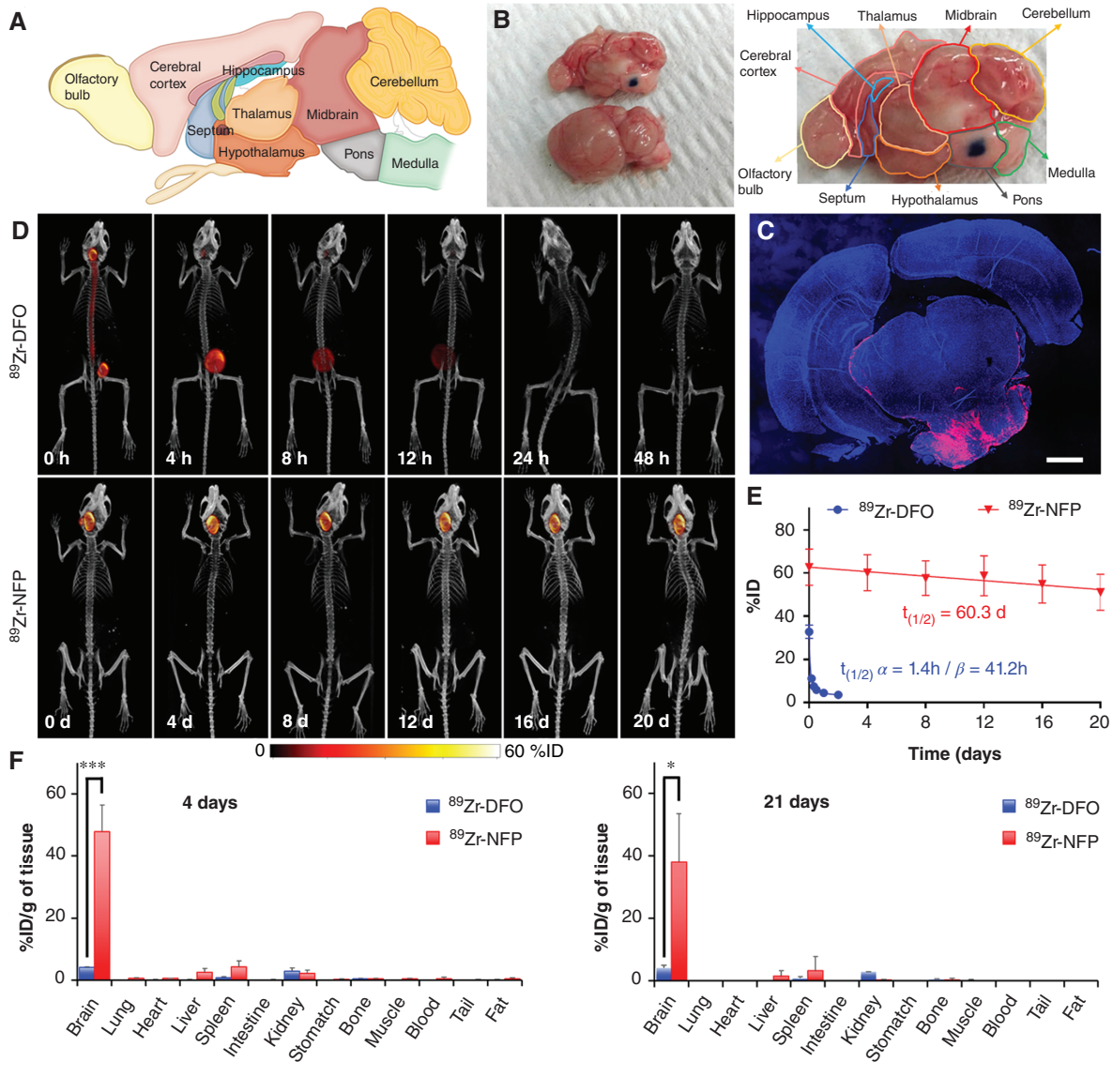

Fig. 2 Post-CED distribution and clearance of ^{89}Zr-NFP. The nanofiber displayed multiple-week-long retention at the CED infusion site. (A) Map showing the different regions and the architecture of a mouse brain (lateral section). (B) Picture showing the successful injection of NFP (plus methylene blue) into the pons via CED. (C) Fluorescence image of a brain section from a representative animal that was euthanized 21 days after ^{89}Zr-NFP infusion (red). DAPI (blue) was used as nuclear staining. Scale bar is 1 mm. (D) Representative whole body PET/CT images of Balb/c mice acquired at various time intervals after CED of ^{89}Zr-NFP or ^{89}Zr-DFO (20 μCi) into the pons (n = 3/group). (E) Plots of the %ID of ^{89}Zr-NFP and ^{89}Zr-DFO in brains over time. The %ID was calculated according to the radioactivity measured at the region of interest (ROI: entire brain) from the acquired PET images. (F) Endpoint biodistribution studies. Separate groups of animals were used for determining the amounts of ^{89}Zr-NFP and ^{89}Zr-DFO uptake by different organs 4 days and 21 days after CED infusion (n = 3/treatment group/time point) (*P < 0.05, **P < 0.01).

saturation and improve the CED/drug treatment outcome. For proof-of-principle studies, we selected DM1 as a model drug candidate. We first synthesized a DM1-conjugated peptide construct via a cleavable disulfide linker (Fig. 3A), sensitive to tumor's reducing environment to release the drug. To achieve this, we introduced the thiol-activated linker succinimidyl 3-(2-pyridyldithio)propionate (SPDP) to the peptide sequence in solid phase. After cleaving the peptide from the resin, DM1 was added to react with the peptide in solution to obtain the final product. We then coassembled Cyanine5.5-labeled, DM1-conjugated, and naïve peptide constructs, at a ratio of 1:4:35, into a DM1-loaded NFP (DM1-NFP) (Fig. 3B, C). At this particular ratio, the nanofiber displayed a minimal fluorescence quenching, allowing us to study the cellular uptake through endocytosis using fluorescence microscopy.[14] As expected, DM1-NFP could be taken up by different glioma cell lines. The cellular uptake of DM1-NFP was time dependent. The Cyanine5.5 fluorescence in the nanofiber-treated cells increased proportionally with time, as shown by FACS analysis (Fig. 3D, E) and

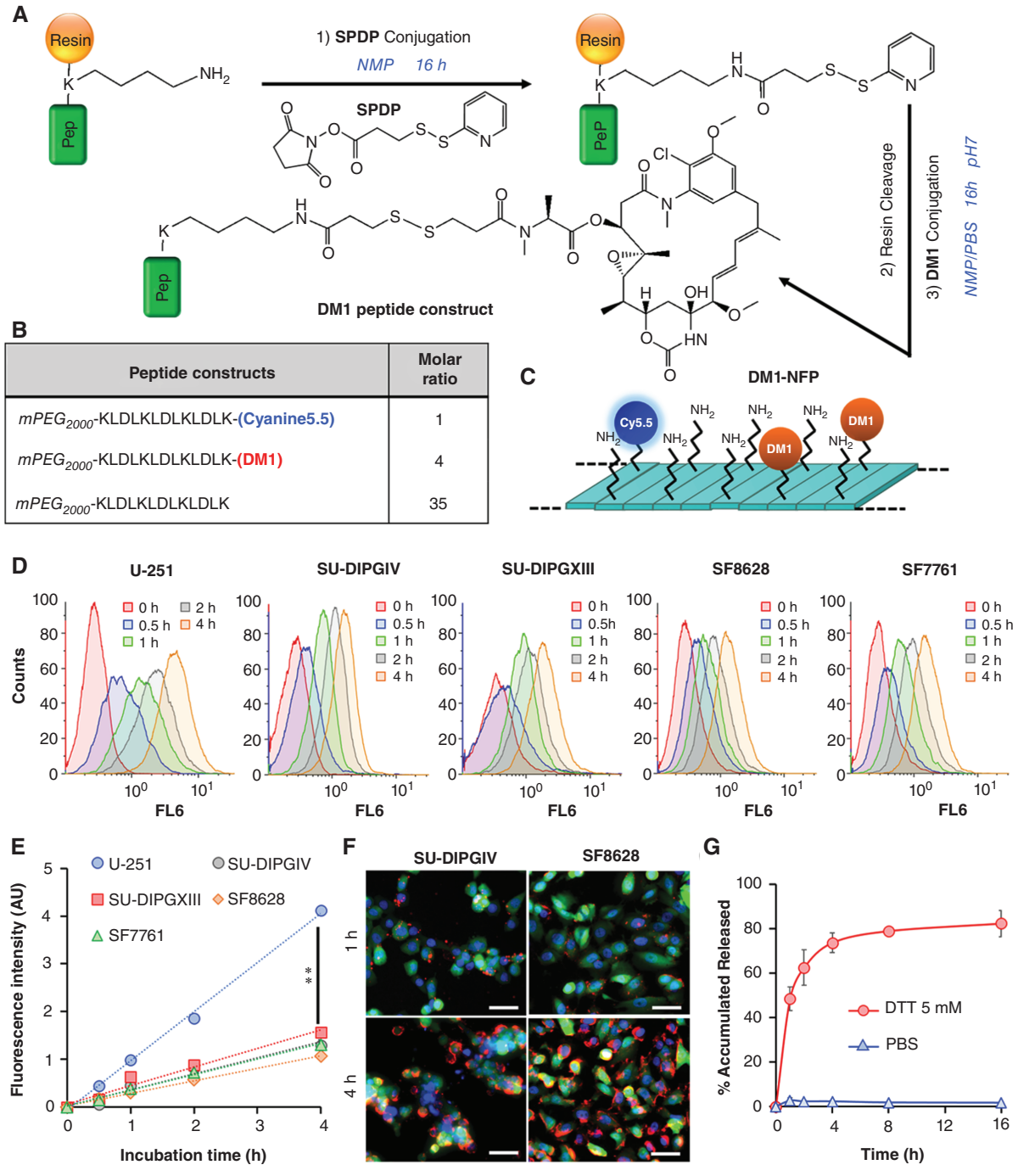

Fig. 3 In vitro cytotoxicity of DM1-NFP. (A) Synthetic scheme of the DM1-conjugated peptide construct. (B) The composition of the DM1-NFP. (C) The nanofiber was coassembled from a mixture of Cyanine5.5-conjugated, DM1-conjugated, and naïve peptide constructs in a ratio of 1:4:35. (D) The cellular uptake of DM1-NFP in SU-DIPGIV, SU-DIPGXIII, U-251, SF8628, and SF7761 human brain cancer cell lines. FACS analysis showing the increase of the intracellular Cy5.5 fluorescence over time. Cells were treated with DM1-NFP (10 μM peptide content) for 0, 0.5, 1, 2, and 4 h prior to FACS analysis. (E) Plots of the kinetics of DM1-NFP cellular uptake by different glioma cell lines. (F) Fluorescence microscopic images showing the cellular uptake of DM1-NFP in glioma cells. Images were acquired 4 h after incubation of DM1-NFP (red, 10 μM peptide content) with GFP/Luc-transduced SU-DIPGIV and SF8628 cells (green). DAPI was added to the cells for staining the nuclei (blue) prior to imaging. Scale bar is 50 μm. (F) DM1-NFP released DM1 in the presence of DTT (5 mM). Plot showing the percentage of accumulated drug release from the nanofiber (10 μM) over time in PBS buffer. The drug release was determined by high-performance liquid chromatography (HPLC) analysis.

imaging studies (Fig. 3F and Supplementary Figure 3). The cellular uptake kinetics and efficiency were similar among all the DIPG cell lines tested. However, the degree of uptake was significantly higher in the case of human glioblastoma astrocytoma (U-251). Importantly, drug release from the nanofiber was triggered by tumor-like conditions generated by reducing agents such as dithiothreitol (DTT) (Fig. 3G and Supplementary Figure 4).[21] For the first time, we showed that DM1 was effective against different glioma cells at nanomolar concentrations. A cell viability assay showed that the cytotoxicity of DM1-NFP was effective against all the cell lines tested (Table 1 and Supplementary Figure 5). DM1-NFP seemed to be less effective against SU-DIPGXIII, with a half-maximal inhibitory concentration (IC_{50}) close to 300 nM. Unlike other cell lines that are monolayer, SU-DIPGXIII was cultured as colonies (3D non-adhesive structures) in suspension (Supplementary Figure 6). Interestingly, DM1-NFP displayed a lower potency against normal brain cells such as astrocytes (IC_{50} value 10–30 times higher), suggesting a selective toxicity of the drug to glioma cell lines. Overall, our results suggested that it was feasible to employ the NFP as a nanocarrier of DM1 while maintaining the cytotoxicity of DM1.

DM1-NFP Displays Superior Therapeutic Efficacy Over Free DM1

Here, we also investigated the therapeutic efficacy of DM1-NFP combined with CED for DIPG treatment. We first orthotopically implanted SU-DIPGIV or SF8628 into the pons of NSG mice. Both cell lines were transduced with GFP and luciferase so that we could monitor glioma progression by bioluminescence imaging (Figures 4A and Supplementary Figure 7A). After 7 days, we randomized the animals and assigned them to DM1-NFP, DM1, or PBS (control) treatment via CED (Fig. 4B). DM1-NFP significantly slowed down the glioma growth compared with free DM1 and PBS in the 2 DIPG models. We observed a decrease of bioluminescence signal at the region of interest (brain) 15 days after treatment (Fig. 4C, D and Supplementary Figure 7B). This was confirmed by a reduction of the average bioluminescence intensity of the animals over time, suggesting that DM1-NFP was able to inhibit DIPG progression. In contrast, the gliomas in animals treated with free DM1 or PBS continued to progress (Fig. 4E and Supplementary Figure 7C). In mice bearing SU-DIPGIV tumor, the ability of DM1-NFP to initially inhibit glioma led to a significant survival benefit. The median survivals of animal groups treated with DM1-NFP, DM1, and PBS were 62 days, 26 days, and 28 days, respectively (Fig. 4F). Furthermore, we did not observe any drug-induced weight loss in animals treated with either DM1 or DM1-NFP (Fig. 4G).

We further confirmed the therapeutic effect of DM1-NFP by histology. The size of gliomas harvested from animals treated with the nanofiber was significantly smaller compared with DM1 and PBS controls (Fig. 5A). Immunohistochemistry analyses revealed that DM1-NFP significantly reduces the percentage of Ki67-immunoreactive cells in the tumor area, suggesting that the drug-loaded nanofibers inhibited both glioma proliferation and growth (Fig. 5B). The therapeutic benefit was attributed to NFP's ability to minimize clearance of DM1 at the infusion site (glioma). We detected the drug was still present in the brains 7 days after CED, as shown by the positive immunoreactivity of primary antibody of DM1 (anti-DM1) (Fig. 5C). The results were also confirmed by LC-MS/MS analysis of the brain extracts. More than 17% of the ID remained in the brains of animals treated with DM1-NFP 7 days after CED. On the other hand, there was only 2% of the ID in the brains of those animals treated with free DM1 (Fig. 5D). Overall, our results showed that DM1-NFP could prolong the drug's local retention, and resulted in enhancement of antiglioma activity compared with DM1, thus indicating great potential for DIPG treatment. To further improve the treatment outcomes and to apply this approach to treat other glioma types, additional studies are required to investigate how the physiochemical makeup of NFP, and CED administration parameters, govern the post-CED distribution and retention and thus the therapeutic efficacy of NFP as a much-needed delivery system.

Table 1 A comparison of the IC_{50} values of DM1 and DM1-NFP tested on different cell lines

IC_{50} (nM)	DM1	DM1-NFP
U-251	9.2 ± 0.9	17.5 ± 2.7
SU-DIPGIV	8.2 ± 1.9	18.3 ± 1.8
SU-DIPGXIII	58.5 ± 13.9	284.4 ± 58.2
SF8628	5.6 ± 0.4	4.9 ± 0.6
SF7761	2.4 ± 0.7	5.9 ± 1.1
Astrocytes	112.3 ± 21.5	161.6 ± 17.8

Discussion

Among all pediatric brain tumors, DIPG is the most morbid. It affects the brainstem and is inoperable. Survival is generally 1 year post-diagnosis, even with radiotherapy. A recent study has shown that primary cultures derived from DIPG patients were sensitive to a number of chemotherapeutics.[22] However, systemic chemotherapy is ineffective against DIPG, even when attempted with drugs that show curative utility in other forms of brain cancer. The BBB of a DIPG patient is normally intact,[23] which prevents most existing and new investigational drugs from reaching the treatment site, the pons, via systemic means. CED is a direct infusion technique that delivers drug-based treatments via surgically implanted catheter.[3] However, there has been limited success applying CED for brain cancer treatment, as drug concentrations quickly decline at treatment sites once infusion stops.[24] Our previous studies showed that NFP effectively extravasated brain tissue and remained locally at the infusion sites (striatum) with a clearance half-life of 57 days.[15,19] We hypothesized that using a combined approach of CED and NFP would increase the local drug delivery and retention, prolong drug-glioma coverage, and maintain an effective (weeks-long) in situ therapeutic concentration for achieving a better treatment outcome.

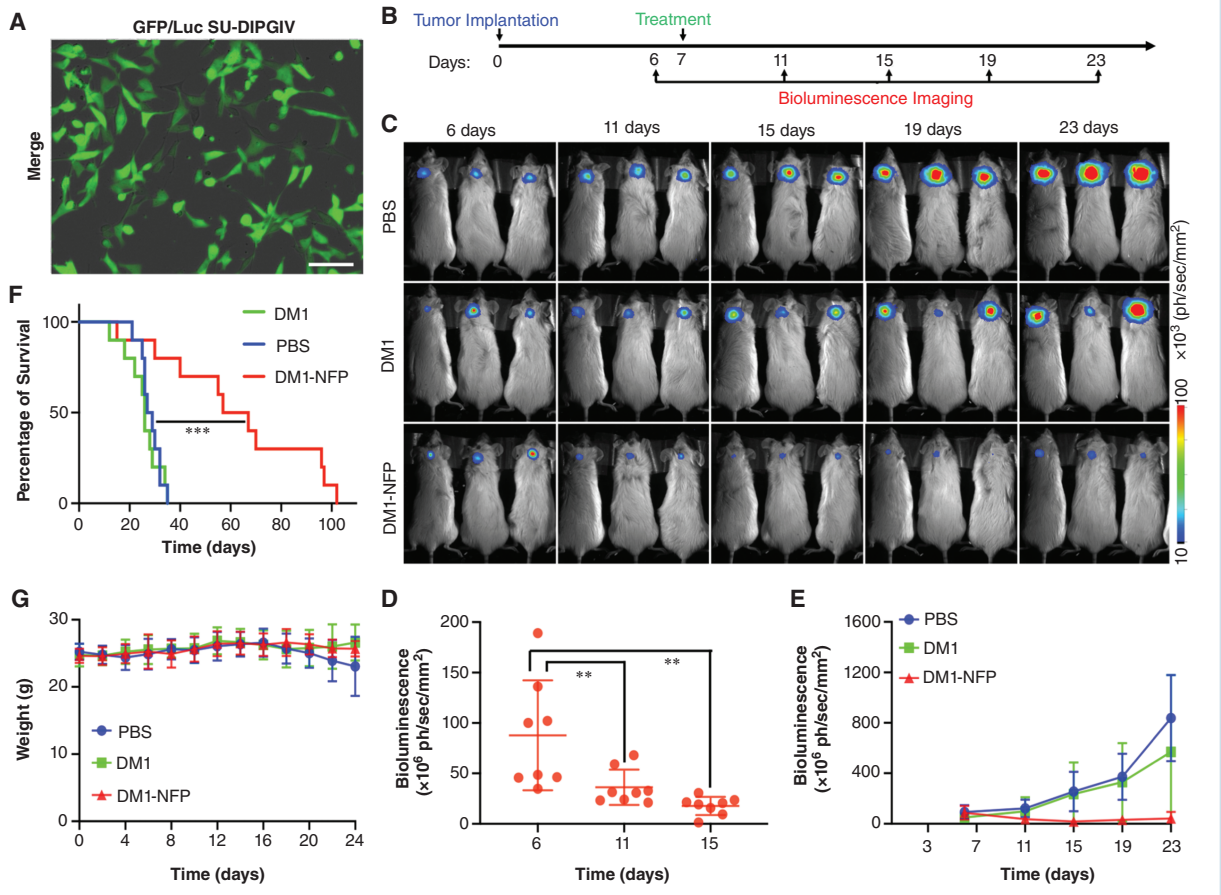

Fig. 4 Therapeutic efficacy of DM1-NFP. (A) A merged bright field and fluorescence image of SU-DIPGIV cell line after transduction with a lentivirus carrying both firefly luciferase and GFP genes. Scale bar is 80 μm. (B) A figure showing the timeline of DIPG implantation, imaging of disease progression, and drug treatment. (C) Representative bioluminescence images of NSG mice bearing orthotopically implanted SU-DIPGIV gliomas at different time intervals after treatment with PBS, free DM1, or DM1-NFP (1 μM; 20 μL) through CED ($n = 10$/group). (D) Animals treated with DM1-NFP showed an initial inhibition of glioma growth. Comparisons of the bioluminescence signals at the region of interest (ROI: entire brain) were made in individual animals within the DM1-NFP treatment group at 6, 11, and 15 days (**$P < 0.01$). (E) A comparison of the bioluminescence signal between animal groups over time. (F) A comparison of the Kaplan–Meier survival rate between the animal groups. The statistical significance was analyzed using the Mantel–Cox log-rank test (***$P < 0.001$). (G) Weight changes of the treated animals. (data do not include animals that did not survive).

We employed NFP as a drug carrier for DIPG treatment. PET/CT imaging study revealed weeks-long retention of ^{89}Zr-labeled NFP in the pons after CED, with a local clearance half-life of 60 days. The local retention property was in agreement with our previous study delivering NFP to the striatum.[15] Importantly, NFP was able to reprofile the biphasic clearance of ^{89}Zr to become linear, providing a more persistent, predictable, and controllable treatment when used as a drug carrier. For the first time, we used the developed NFP as a carrier of DM1. DM1 is the drug component of many antibody-drug conjugates. Instead of using a targetable antibody as carrier of DM1 through systemic (intravenous) administration, we incorporated DM1 into NFP for treating DIPG via CED. As mentioned above, DIPG is an untreatable lethal condition. A slight improvement in patient survival would make a clinical impact on DIPG treatment. Here, the drug-loaded NFP (DM1-NFP) was associated with a significant improvement in treatment outcome compared with free DM1. DM1-NFP doubled the median survival of animals bearing DIPG compared with free DM1 and PBS treatments. Interestingly, DM1-NFP was capable of initially reducing DIPG, but the glioma slowly regressed. The animals were treated with only a single NFP infusion with a small amount of drug (15 ng/mouse). To optimize the treatment, further studies are needed to investigate how the nanofiber's drug payload and dosage (including number of infusions) as well as other CED parameters, such as administration flow rate and volume, impact the therapeutic outcome and toxicity. Overall, we established a combined CED and NFP approach to overcome major drug delivery barriers in the brain. This approach should have far-reaching potential to reduce administration dosage, injection volume, and inpatient time, minimizing risks of admission-associated infection, mechanical injury, and systemic toxicity. The design flexibility of the NFP should permit incorporation of other radioisotopes (for local radiotherapy administration) in the future.

DIPG is a heterogeneous disease, and is categorized into 3 molecular subgroups: H3K27M, MYCN, and Silent.[25]

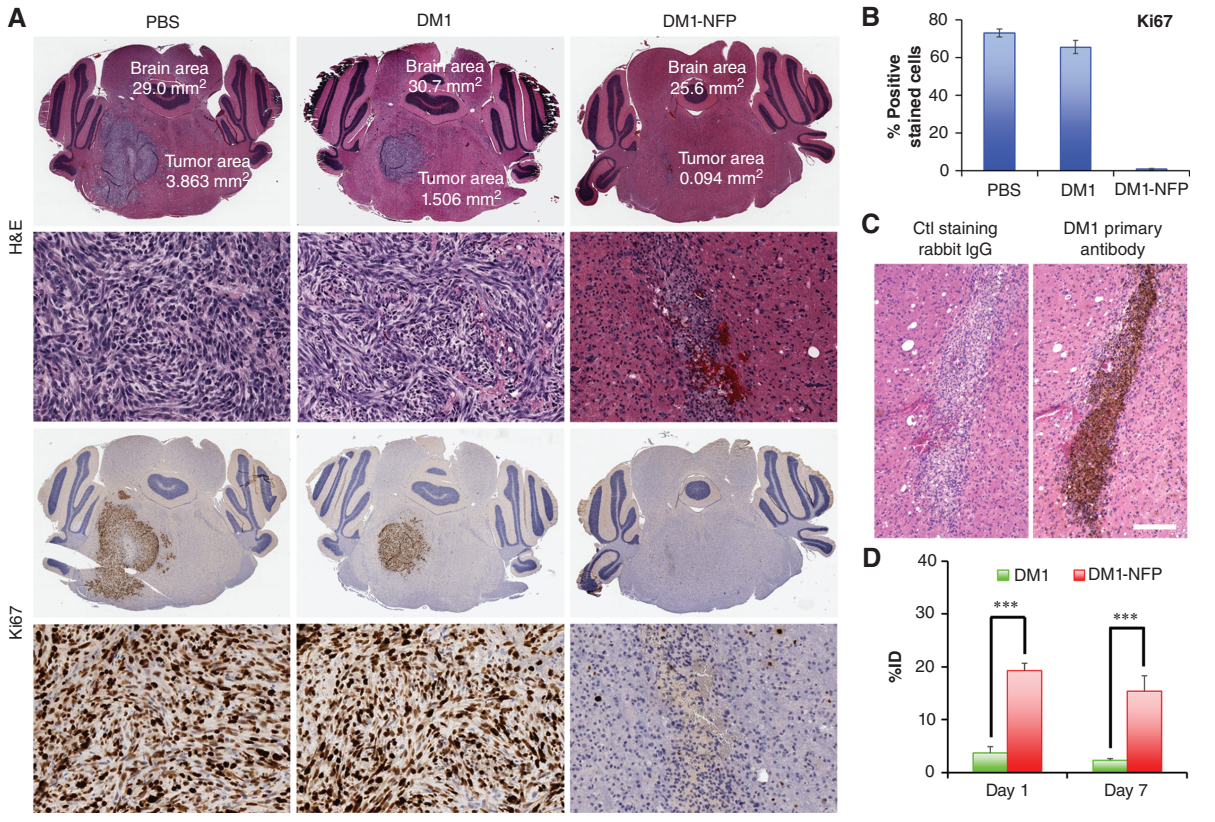

Fig. 5 (A) Representative brain sections of animals after treatments with PBS, free DM1 (1 μM), or DM1-NFP (1 μM of drug content; 20 μL) via CED. The brains were harvested 14 days after the corresponding treatments. The brains were then paraffin-embedded, sectioned, and stained with H&E, and Ki67 (proliferation marker). (B) Graph bars showing the proportion of Ki67 immunoreactive cells in the tumor area after treatment with PBS, free DM1, or DM1-NFP. (C) Immunohistochemistry confirmed that DM1 was present in the brain sections of animals treated with DM1-NFP. The drug was detected using primary antibody against DM1 (left). Rabbit IgG was used as negative control antibody (right). Scale bar is 400 μm. (D) A comparison of %ID remaining in the brains of animals treated with DM1 and DM1-NFP (15 ng of drug content) after CED. Separate groups of animals were used for this study. At day 1 or day 7 after the treatments ($n = 4$/treatment/time point), the animals were euthanized. The brain extracts were collected and analyzed for the amount of drug content using the LC-MS/MS method (**$P < 0.01$, ***$P < 0.001$).

H3K27M is the most common one. More than 80% of DIPGs harbor H3 K27M mutation.[26] The MYCN subgroup has no recurrent mutation, and is characterized with hypermethylation and *MCYN* amplification. The Silent subgroup has a lower mutation rate but overexpresses *MDM2*, *MSMP*, and *ADAM33*. Demethylase inhibitor (eg, GSKJ4) and histone deacetylase inhibitor (eg, panobinostat) have been proposed as epigenetic therapies for DIPG.[27] DIPG displays histologic intratumoral heterogeneity in H3 K27M mutation and H3 K27 trimethylation.[28] In addition, 56% of the histology showed focal areas reassembling World Health Organization grade I tumors (pilocytic astrocytoma and subependymoma). The inter- and intratumoral heterogeneity nature of DIPG suggests that multiple drugs with distinctive mechanisms of action are needed to control the disease progression. DM1 is a tubulin inhibitor. It is more potent compared with other chemotherapeutics, and should be effective against DIPG regardless of the specific point mutations or epigenetic changes (molecular subgroups) of the glioma.[25] We foresee that the developed DM1-NFP can be used together with epigenetic therapies to provide a comprehensive and effective DIPG treatment.

Supplementary Material

Supplementary data are available at *Neuro-Oncology* online.

Keywords

convection-enhanced delivery | diffuse intrinsic pontine glioma | emtansine | peptide nanofiber

Funding

This research work was supported in part by the National Cancer Institute (R01 CA222802 to B.L.), the US Department of Defense (CA160373 to B.L.), and the Weill Cornell Medicine, Radiology Department.

Acknowledgments

The authors would like to thank the Memorial Sloan Kettering Radiochemistry and Molecular Imaging Probe Core Facility for supplying ^{89}Zr-oxylate. The facility was supported in part through the NIH/NIC Cancer Center Support Grant (P30 CA008748). The authors would like to thank the Electron Microscopy and Histology Core Facility in Weill Cornell Medicine for help with transmission electron microscopy and tissue sections, as well as the Flow Cytometry Core Facility for performing cell sorting experiments. The authors also acknowledge the Laboratory of Comparative Pathology Core Facility in MSKCC, partially funded by NCI grant P30 CA008748, for the immunohistochemistry of the brain sections. The authors would also like to thank Hanan Alwaseem from Proteomic Resource Center, Rockefeller University, for assisting LC/MS-MS experiments. Finally, the authors would also thank Cynthia Fox for the editing of this manuscript.

Conflict of interest statement. The authors declare no competing interests.

Authorship statement. V. Bellat and B. Law initiated the study and the conceptual design of the experiments. V. Bellat performed the design, synthesis, in vitro characterization, drug release study of NFP, imaging, and the data analysis. She also proofread the manuscript. Y. Alcaina performed PET imaging, biodistribution, and survival studies, and assisted with the LC-MS/MS analysis, and histology. A. Michel performed the histological analysis. R. Ting assisted in PET/CT imaging. C-H. Tung and M. Souweidane provided technical advice and assistance. V. Bellat and Y. Alcaina prepared the manuscript. B. Law proofread the manuscript, conceived the study, secured the funding, and supervised the entire project.

References

1. Hargrave D, Bartels U, Bouffet E. Diffuse brainstem glioma in children: critical review of clinical trials. *Lancet Oncol.* 2006;7(3):241–248.
2. Johung TB, Monje M. Diffuse intrinsic pontine glioma: new pathophysiological insights and emerging therapeutic targets. *Curr Neuropharmacol.* 2017;15(1):88–97.
3. Zhou Z, Singh R, Souweidane MM. Convection-enhanced delivery for diffuse intrinsic pontine glioma treatment. *Curr Neuropharmacol.* 2017;15(1):116–128.
4. Vanan MI, Eisenstat DD. DIPG in children—what can we learn from the past? *Front Oncol.* 2015;5:237.
5. Lapin DH, Tsoli M, Ziegler DS. Genomic insights into diffuse intrinsic pontine glioma. *Front Oncol.* 2017;7:57.
6. Sewing AC, Caretti V, Lagerweij T, et al. Convection enhanced delivery of carmustine to the murine brainstem: a feasibility study. *J Neurosci Methods.* 2014;238:88–94.
7. Singleton WGB, Bienemann AS, Woolley M, et al. The distribution, clearance, and brainstem toxicity of panobinostat administered by convection-enhanced delivery. *J Neurosurg Pediatr.* 2018;22(3):288–296.
8. Noble CO, Krauze MT, Drummond DC, et al. Novel nanoliposomal CPT-11 infused by convection-enhanced delivery in intracranial tumors: pharmacology and efficacy. *Cancer Res.* 2006;66(5):2801–2806.
9. Shahar T, Ram Z, Kanner AA. Convection-enhanced delivery catheter placements for high-grade gliomas: complications and pitfalls. *J Neurooncol.* 2012;107(2):373–378.
10. Valles F, Fiandaca MS, Bringas J, et al. Anatomic compression caused by high-volume convection-enhanced delivery to the brain. *Neurosurgery.* 2009;65(3):579–585; discussion 585–586.
11. Bander ED, Tizi K, Wembacher-Schroeder E, et al. Deformational changes after convection-enhanced delivery in the pediatric brainstem. *Neurosurg Focus.* 2020;48(1):E3.
12. Corem-Salkmon E, Ram Z, Daniels D, et al. Convection-enhanced delivery of methotrexate-loaded maghemite nanoparticles. *Int J Nanomedicine.* 2011;6:1595–1602.
13. Danhier F, Messaoudi K, Lemaire L, Benoit JP, Lagarce F. Combined anti-Galectin-1 and anti-EGFR siRNA-loaded chitosan-lipid nanocapsules decrease temozolomide resistance in glioblastoma: in vivo evaluation. *Int J Pharm.* 2015;481(1-2):154–161.
14. Bellat V, Ting R, Southard TL, et al. Functional peptide nanofibers with unique tumor targeting and enzyme-induced local retention properties. *Adv Funct Mater.* 2018;28(44).
15. Tosi U, Kommidi H, Bellat V, et al. Real-time, in vivo correlation of molecular structure with drug distribution in the brain striatum following convection enhanced delivery. *ACS Chem Neurosci.* 2019;10(5):2287–2298.
16. Chariou PL, Lee KL, Pokorski JK, Saidel GM, Steinmetz NF. Diffusion and uptake of tobacco mosaic virus as therapeutic carrier in tumor tissue: effect of nanoparticle aspect ratio. *J Phys Chem B.* 2016;120(26):6120–6129.
17. Law B, Weissleder R, Tung CH. Protease-sensitive fluorescent nanofibers. *Bioconjug Chem.* 2007;18(6):1701–1704.
18. Wagh A, Singh J, Qian S, Law B. A short circulating peptide nanofiber as a carrier for tumoral delivery. *Nanomedicine.* 2013;9(4):449–457.
19. Singh R, Bellat V, Wang M, et al. Volume of distribution and clearance of peptide-based nanofiber after convection-enhanced delivery. *J Neurosurg.* 2018;129(1):10–18.
20. Rosenthal M, Curry R, Reardon DA, et al. Safety, tolerability, and pharmacokinetics of anti-EGFRvIII antibody-drug conjugate AMG 595 in patients with recurrent malignant glioma expressing EGFRvIII. *Cancer Chemother Pharmacol.* 2019;84(2):327–336.
21. Erickson HK, Widdison WC, Mayo MF, et al. Tumor delivery and in vivo processing of disulfide-linked and thioether-linked antibody-maytansinoid conjugates. *Bioconjug Chem.* 2010;21(1):84–92.
22. Veringa SJ, Biesmans D, van Vuurden DG, et al. In vitro drug response and efflux transporters associated with drug resistance in pediatric high grade glioma and diffuse intrinsic pontine glioma. *PLoS One.* 2013;8(4):e61512.
23. Subashi E, Cordero FJ, Halvorson KG, et al. Tumor location, but not H3.3K27M, significantly influences the blood-brain-barrier permeability in a genetic mouse model of pediatric high-grade glioma. *J Neurooncol.* 2016;126(2):243–251.
24. Kommidi H, Tosi U, Maachani UB, et al. 18F-radiolabeled panobinostat allows for positron emission tomography guided delivery of a histone deacetylase inhibitor. *ACS Med Chem Lett.* 2018;9(2):114–119.
25. Buczkowicz P, Hoeman C, Rakopoulos P, et al. Genomic analysis of diffuse intrinsic pontine gliomas identifies three molecular subgroups and recurrent activating ACVR1 mutations. *Nat Genet.* 2014;46(5):451–456.
26. Wu G, Diaz AK, Paugh BS, et al. The genomic landscape of diffuse intrinsic pontine glioma and pediatric non-brainstem high-grade glioma. *Nat Genet.* 2014;46(5):444–450.
27. Hashizume R. Epigenetic targeted therapy for diffuse intrinsic pontine glioma. *Neurol Med Chir (Tokyo).* 2017;57(7):331–342.
28. Bugiani M, Veldhuijzen van Zanten SEM, Caretti V, et al. Deceptive morphologic and epigenetic heterogeneity in diffuse intrinsic pontine glioma. *Oncotarget.* 2017;8(36):60447–60452.